

Calculation of Altitude-Dependent Tikhonov Constraints for TES Nadir Retrievals

Susan Sund Kulawik, Gregory Osterman, Dylan B. A. Jones, and Kevin W. Bowman

Abstract—A key component in the regularization of vertical atmospheric trace gas retrievals is the construction of constraint matrices. We introduce a novel method for developing a constraint matrix based on altitude-varying combinations of zeroth-, first-, and second-order derivatives of the trace gas profile. This constraint matrix can be optimized to minimize the diagonal *a posteriori* error covariance and can also consider other factors such as degrees of freedom. This approach is applied to the calculation of constraint matrices for Tropospheric Emission Spectrometer nadir retrievals of atmospheric temperature, H₂O, O₃, CO, and CH₄. The retrieval error achieved with these constraints is comparable to the error achieved with the classical Bayesian constraint. Furthermore, these constraints are shown to be robust under uncertainty in the climatological conditions.

Index Terms—EOS-Aura, error analysis, infrared remote sensing, Fourier transform spectrometry (FTS), nonlinear estimation, Tropospheric Emission Spectrometer (TES).

I. INTRODUCTION

CONSTRAINTS are used to regularize an ill-posed problem to obtain a stable solution that is an approximation to the exact solution [1]. Constraints that are too strong will characteristically yield a stable, though inaccurate solution which has more *a posteriori* error, fewer degrees of freedom (DOF), and less resolution than an optimal retrieval; whereas constraints that are too weak will characteristically result in instability with more *a posteriori* error, although appear to have more DOF and better resolution than an optimal retrieval. Standard constraints for atmospheric retrievals include the inverse of a climatology and Tikhonov constraints. However, each of these has some properties that can be suboptimal. Climatological constraints may include undesirable characteristics, such as containing correlations between the stratosphere and troposphere, being finely tuned to a particular climatology, and not being optimized for the inclusion of systematic error. Tikhonov constraints of a single type or with a single strength value can introduce error because different strengths and types may be more appropriate for different parts of the atmosphere.

The Tropospheric Emission Spectrometer (TES) is an infrared Fourier transform spectrometer designed to study the Earth's ozone, air quality, and climate on the EOS-Aura

platform¹ [4]. Choosing constraints used for TES retrievals of atmospheric temperature (T_{atm}), water vapor (H₂O), ozone (O₃), carbon monoxide (CO), and methane (CH₄) is the subject of this paper.

A. Motivation

Under the assumption that the atmospheric state can be described by a Gaussian process with a known climatological covariance, the constraint matrix that minimizes the *a posteriori* error of the estimate is the inverse of that climatological covariance, hereafter referred to as the "climatological constraint." However, the climatological constraint may not be robust given uncertainty resulting from systematic errors and actual climatological conditions.

Consequently, in the course of TES spectral window selection, constraint selection, and tests with simulated data, it was found that the direct use of the climatological constraint was not sufficiently robust, as discussed in Sections I-A1–A3.

1) *The Global Atmosphere Has Uncertain Statistics:* For the climatological constraint to be the optimal constraint, the retrieval dataset must have identical statistics to the climatology used. TES is measuring an atmosphere where the actual climatology is variable and uncertain, especially for less-studied species. Considering DOF in constraint selection, described later in this paper, can hedge against these unknowns by encouraging the constraint selection to retain DOF in spite of low variability, and therefore be more prepared for unexpected climatological conditions.

2) *TES Has Systematic Errors:* For the climatological constraint to be the best constraint, the systematic errors must not be significant. TES errors are dominated by smoothing error, however the systematic error from temperature and water vapor is not insignificant for ozone retrievals, and line-parameter error is not insignificant for water vapor, temperature, and ozone retrievals [3]. Von Clarmann *et al.* [6] have proposed a method to include systematic errors in the off-diagonal radiance noise, however TES does not currently use this retrieval method, whereas constraint modification can be used within our current retrieval framework.

3) *Climatological Covariances Available to TES Are Not Always Invertible, Positive Definite, and With Reasonable Condition Numbers:* Covariances created from MOZART [12], [13] profiles from one day (described in Section III-E) were not always positive definite, meaning that some combinations of errors can create negative additions to the cost function (i.e., appear better than the true state).

Manuscript received April 22, 2005; revised December 6, 2005. This work was conducted by the Jet Propulsion Laboratory, California Institute of Technology, under a contract with the National Aeronautics and Space Administration.

S. S. Kulawik, G. Osterman, and K. W. Bowman are with the Jet Propulsion Laboratory, Pasadena, CA 91109 USA (e-mail: Susan.Sund.Kulawik@jpl.nasa.gov).

D. B. A. Jones is with the Department of Physics, University of Toronto, Toronto, ON M5S 1A7, Canada.

Digital Object Identifier 10.1109/TGRS.2006.871206

¹<http://aura.gsfc.nasa.gov>

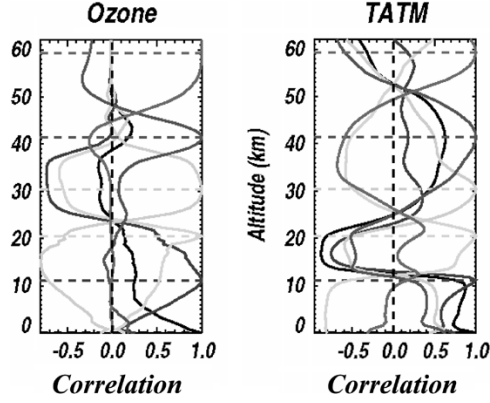


Fig. 1. Ozone and atmospheric temperature correlations between different altitudes in MOZART data. Various rows of the correlation matrix ($\text{covariance}_{ij}/\sqrt{\text{covariance}_{ii}\sqrt{\text{covariance}_{jj}}}$) are plotted; the horizontal dotted lines show the altitude for each plotted row and the vertical black dotted line shows 0 correlation. Note the long-scale correlations and anticorrelations throughout all altitudes. When the inverse climatology is used as a constraint, the same long-scale correlations and anticorrelations will be introduced into the retrieval results.

4) *Climatological Covariances Available to TES Can Have Unwanted Correlations*: Long-scale correlations exist in our MOZART covariances (see Fig. 1), e.g., between the troposphere and stratosphere, which may be appropriately correlated in the model. However, if the inverse of such a climatology were used as a constraint for TES retrievals, it would introduce the same long-scale correlations in the retrieval results and may indicate sensitivities where none may exist. A climatology could be modified to remove long-scale oscillatory correlations by fitting correlations to an exponential decay, for example, before the covariance is inverted for use as a constraint. Similarly, the constraint selection described in this paper can be thought of as a type of covariance modeling technique.

II. THEORY

A. Evaluating Constraints

The purpose of this section is to develop a method for evaluating the quality of a constraint. The expected error covariance for retrieving an ensemble of true states is developed in Section II-B1. This error covariance, which depends on the constraint, is then evaluated by using metrics developed in Section II-B2. This is used to find the best constraint. First, however, brief descriptions of the forward model and inversion problems must be given; for more details on these topics, see [2]–[5].

1) *Forward Model*: From the perspective of the retrieval of the atmospheric state, the forward model is a function that deterministically maps from an atmospheric state \mathbf{x} to a radiance $\mathbf{L}(\mathbf{x})$. The observed state \mathbf{L}_{obs} is a discretized vector and is related to the true state radiance $\mathbf{L}(\mathbf{x}, \mathbf{b})$ by an additive noise model

$$\mathbf{L}_{\text{obs}} = \mathbf{L}(\mathbf{x}, \mathbf{b}) + \varepsilon \quad (1)$$

where ε is the measurement noise, \mathbf{x} is the true state, and \mathbf{b} are the true values for parameters that are not retrieved but are used in the forward model generation (such as nonretrieved trace

gases). The Jacobian \mathbf{K} tells how the radiance changes with respect to a state parameter

$$\mathbf{K}_{ij}^x = \partial \mathbf{L}_i / \partial x_j. \quad (2)$$

2) *Cost Function*: The cost function used by TES, χ^2 , is defined [5]

$$\chi^2 = \|\mathbf{L}_{\text{obs}} - \mathbf{L}(\mathbf{z}, \hat{\mathbf{b}})\|_{\mathbf{S}_m}^2 + \|\mathbf{z}_{\text{apriori}} - \mathbf{z}\|_{\Lambda}^2 \quad (3)$$

where $\mathbf{L}(\mathbf{z}, \hat{\mathbf{b}})$ is the radiance at the current state; $\mathbf{S}_m = \langle (\varepsilon - \bar{\varepsilon})(\varepsilon - \bar{\varepsilon})^T \rangle$ is the data noise covariance; \mathbf{z} , is the vector of retrieved parameters, Λ is a constraint matrix, and note that $\|\mathbf{x}\|_{\Lambda}^2 \equiv \mathbf{x}^T \Lambda \mathbf{x}$. The state \mathbf{x} is on a finer-scale grid needed for forward model computations and is related to retrieval parameters \mathbf{z} by

$$\mathbf{x} = \mathbf{M}\mathbf{z} \quad (4)$$

where \mathbf{M} maps from the retrieved parameters \mathbf{z} to the state \mathbf{x} . This cost function is at a minimum when the retrieved parameters \mathbf{z} result in a close match between $\mathbf{L}(\mathbf{z}, \hat{\mathbf{b}})$ and the observed radiance \mathbf{L}_{obs} and the parameters \mathbf{z} are close to $\mathbf{z}_{\text{apriori}}$, where “close” is defined by a constraint. The cost function χ^2 can be minimized to find the best retrieval parameters using a nonlinear least squares retrieval.

3) *Expected Ensemble Error Covariance*: The expected errors for an ensemble of retrieved states can be calculated if we have knowledge of our data error variability, the state variability, as well as the dependence of the forward model on our retrieved parameters \mathbf{K} described in Section II-A1. This expected error can then be used to select spectral windows [3], retrieval parameters, retrieval strategies, and select constraints as discussed in this paper. The limitations are that Gaussian statistics and additive noise are assumed, and it is assumed that the nonlinear retrieval is able to converge to the global rather than a local minimum.

The development of the expected ensemble error covariance is developed in Rodgers [2]. First, the modeled radiance is expanded linearly from the true state radiance

$$\mathbf{L}(\hat{\mathbf{z}}, \hat{\mathbf{b}}) = \mathbf{L} + \mathbf{K}^x [\mathbf{M}\hat{\mathbf{z}} - \mathbf{x}_{\text{true}}] + \mathbf{K}^b [\hat{\mathbf{b}} - \mathbf{b}_{\text{true}}] \quad (5)$$

where $\hat{\mathbf{z}}$ are the retrieved parameters, $\hat{\mathbf{b}}$ are estimates of unretrieved parameters, \mathbf{L} is the radiance, \mathbf{M} is a map between \mathbf{z} and \mathbf{x} , the full state (4), and \mathbf{K} is the Jacobian (2).

Equations (5) and (1) are substituted into (3), and solved for the optimal retrieved state $\hat{\mathbf{z}}$ using $\Sigma d\chi^2/dz = 0$. The solution for $\hat{\mathbf{z}}$ is then mapped back to the full state grid using (4) to get the retrieved state solution

$$\hat{\mathbf{x}} = \mathbf{M}\mathbf{z}_{\text{apriori}} + \mathbf{M}\mathbf{G}^z \mathbf{K} [\mathbf{x}_{\text{true}} - \mathbf{M}\mathbf{z}_{\text{apriori}}] + \mathbf{M}\mathbf{G}^z \varepsilon + \mathbf{M}\mathbf{G}^z \mathbf{K}^b [\hat{\mathbf{b}} - \mathbf{b}_{\text{true}}],$$

where $\mathbf{G} = (\mathbf{K}^{zT} \mathbf{S}_m^{-1} \mathbf{K}^z + \Lambda)^{-1} \mathbf{K}^{zT} \mathbf{S}_m^{-1}$. The error covariance is defined as

$$\mathbf{S}_{\text{error}} \equiv \langle (\mathbf{x}_{\text{true}} - \hat{\mathbf{x}})(\mathbf{x}_{\text{true}} - \hat{\mathbf{x}})^T \rangle$$

If we have knowledge about the expected variability of our initial state (\mathbf{S}_a), then the expected error of our retrieved state is

$$\mathbf{S}_{\text{error}} = \|\mathbf{I} - \mathbf{M}\mathbf{G}^z \mathbf{K}^x\|_{\mathbf{S}_a}^2 + \|\mathbf{M}\mathbf{G}^z\|_{\mathbf{S}_m}^2 + \|\mathbf{M}\mathbf{G}^z \mathbf{K}^b\|_{\mathbf{S}_b}^2 \quad (6)$$

Equation (6) is used to develop optimal constraints in this paper and can also be used to select optimal spectral windows, as shown by [3] and could be used to choose optimal retrieval parameterization.

B. Metrics

The error covariance (6) is too complex to evaluate. Judging between two error covariances as to which is “better” is impossible without development of single-value metrics. Three metrics are used to judge a constraint’s performance.

- *DOF for data.* The DOF is a measure of how many retrieved parameters or fractions of parameters come from the data rather than the *a priori*

$$\text{DOF} = \sum_i \mathbf{A}_{ii} = (\mathbf{G}^z \mathbf{K}^x)_{ii}$$

where \mathbf{A} is the “Averaging kernel” [2], [7]. Note that \mathbf{A} does not depend on the choice of \mathbf{S}_a , the *a priori* uncertainty of the atmosphere. It does, of course, depend on the constraint choice (as discussed in [9]).

- *Mean error.* The mean error is the root-mean-square of the errors for all the state parameters

$$\bar{\sigma} = \sqrt{\text{Trace}(\mathbf{S}_{\text{error}})/n} \quad (7)$$

where n is the number of state parameters. This metric is used by [9] for determining a constraint strength.

- *Resolution at 500 mB.* This is the full-width half-maximum for the row of \mathbf{A} at 500 mb; this is used because this is the only altitude where all species have a relatively well-defined vertical resolution. Since this metric only considers one part of the atmosphere, it does not track problems or improvements at other levels and so it is not used for constraint selection. For example, a constraint that substantially improves error in the upper troposphere but slightly worsens the resolution at 500 mb would be penalized by this metric.

C. Figures of Merit

Two figures of merit were used:

- Minimizing the mean error, defined in (7).
- Minimizing mean error/DOF^{1/8}. The value 1/8 was selected using the study shown in Fig. 4. The DOF component is used to encourage the constraint to retain DOF when it did not unduly adversely affect the errors.

One other figure of merit was considered but ultimately rejected, which is to maximize “bits” [2], [3], defined

$$\text{bits} = \frac{1}{2}(\log_2 |\mathbf{S}_a| - \log_2 |\mathbf{S}_{\text{error}}|).$$

This figure of merit was not used in this paper because $|\mathbf{S}_{\text{error}}|$ was in many cases very small ($<10^{-300}$) and numerically unstable when computed on the full state grid as was done in this paper, rather than the retrieval grid as was done by [3].

D. Constraint Composition and Solution

A constraint framework was chosen to limit the number of tunable parameters in the constraint. For example, if all values for the constraint for TES temperature, which has 25 retrieved parameters, were allowed to separately vary, this would result

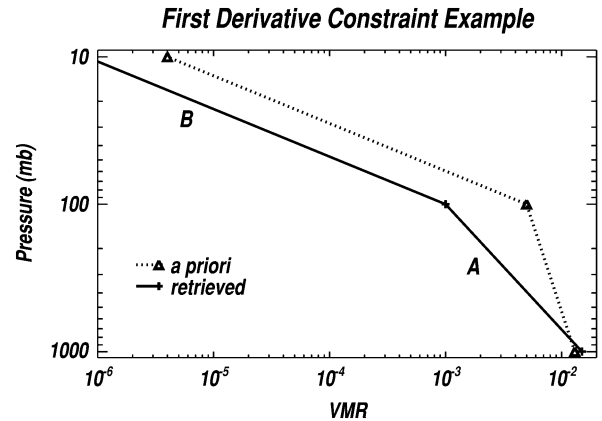


Fig. 2. Altitude-dependent constraint example. The first derivative (slope) of the retrieved water vapor VMR (solid) is constrained by the first derivative (slope) of the *a priori* (dotted line) using an altitude-dependent first derivative constraint. In this example, the slope of *B* is heavily constrained and the slope of *A* is allowed to vary.

in 625 tunable parameters. In contrast, a zeroth derivative Tikhonov constraint allows only 25 tunable parameters.

Tikhonov constraints were chosen as a well-characterized framework in which to develop the more specialized constraints. Tikhonov constraints are an *ad hoc* regularization [8] that can be applied to atmospheric retrievals [9]. Tikhonov constraints add a term to the cost function which penalizes deviations from the zeroth, first and/or second derivative of the *a priori* profile; only when there is enough information to overcome this penalty does the parameter deviate from the *a priori* characteristics. Combinations of zeroth, first, and second derivative Tikhonov constraints have been previously used, although with just one scalar parameter to weight each constraint type [10]

$$\text{constraint} = a\mathbf{L}^{(0)} + b\mathbf{L}^{(1)} + c\mathbf{L}^{(2)}$$

where $\mathbf{L}^{(1)}$ represents the first derivative constraint. Steck [9] introduced methods for determining a single constraint strength for Tikhonov constraints by optimizing a figure of merit, such as the mean error for an ensemble of profiles. In this way, Steck used *a priori* information to determine the best single parameter to use for Tikhonov constraints. This paper extends this approach to select altitude-dependent constraint strengths with combinations of zeroth, first, and second derivative Tikhonov constraints.

1) *Altitude-Dependent Tikhonov Constraints:* Altitude-dependent constraint strengths are created by breaking up a Tikhonov constraint into the smallest constrainable units, each of which may have a different strength. For example, in Fig. 2, separate first derivative constraints can be used to constrain the slopes for segments *A* and *B*. The 3×3 constraint used for this retrieval example could be described by (8) with $\mathbf{a} = [0, 0, 0]$, $\mathbf{b} = [\text{small number}, \text{large number}]$, and $\mathbf{c} = [0]$. Constraining different parts of the atmosphere differently is useful when sensitivity varies with altitude.

2) *Penalty Terms for Derivative Constraints:* Derivative constraints penalize the derivatives of the difference between the state and the *a priori* value ($\mathbf{x} - \mathbf{x}_a$) in the cost function (3). The zeroth derivative constrains the value, the first derivative constrains the slope, and the second derivative constrains the

curvature of the result. The derivative operator can be expressed as a matrix multiplier, \mathbf{D} , and the magnitude of the derivative of $(\mathbf{x} - \mathbf{x}_a)$ can then be written $\|\mathbf{D}(\mathbf{x} - \mathbf{x}_{\text{apriori}})\|^2$. This penalty term is of the same form as the second term of the cost function in (3) with the constraint matrix set to

$$\Lambda = \mathbf{D}^T \mathbf{D}.$$

The derivative matrix $\mathbf{D}^{n,i}$, representing the n th order (zeroth, first, or second) derivative at the i th altitude, is a matrix that is zero except for the partial row vector $\mathbf{d}^{(n)}$ starting at the $(i$ th, i th) position, where the $\mathbf{d}^{(n)}$ partial row vectors are

$$\begin{aligned} \mathbf{d}^{(0)} &= (1) \\ \mathbf{d}^{(1)} &= (1 \quad -1) \\ \mathbf{d}^{(2)} &= (-1 \quad 2 \quad -1). \end{aligned}$$

The constraint matrix corresponding to $\mathbf{D}^{n,i}$ is $\Lambda^{n,i} = (\mathbf{D}^{n,i})^T \mathbf{D}^{n,i}$. Each of the derivative matrices $\Lambda^{n,i}$ can be individually weighted and combined to create a constraint that constrains the zeroth, first, and second derivatives of all parts of the atmosphere, with the relative and absolute strengths depending on the magnitudes of \mathbf{a} , \mathbf{b} , and \mathbf{c}

$$\Lambda = \sum_{i=0}^{n-1} \mathbf{a}_i \Lambda^{0,i} + \sum_{i=0}^{n-2} \mathbf{b}_i \Lambda^{1,i} + \sum_{i=0}^{n-3} \mathbf{c}_i \Lambda^{2,i}. \quad (8)$$

$\Lambda^{1,0}$, $\Lambda^{1,n-2}$, $\Lambda^{2,0}$, and $\Lambda^{2,n-3}$ are modified slightly because these constrain end points less than interior points. Since constraint strengths are constrained to smoothly vary with altitude in the next section, diagonal values were added to make a uniform value along the diagonal when the constraint weights are identical. For example, the modified $\Lambda^{1,0}$ and $\Lambda^{1,3}$ matrices for a 4×4 constraint are

$$\Lambda^{1,0} = \begin{pmatrix} 2 & -1 & 0 & 0 \\ -1 & 1 & 0 & 0 \\ 0 & 0 & 0 & 0 \\ 0 & 0 & 0 & 0 \end{pmatrix}$$

$$\Lambda^{1,3} = \begin{pmatrix} 0 & 0 & 0 & 0 \\ 0 & 0 & 0 & 0 \\ 0 & 0 & 1 & -1 \\ 0 & 0 & -1 & 2 \end{pmatrix}.$$

3) *Polynomial Dependence of Strength Parameters*: The number of \mathbf{a} , \mathbf{b} , and \mathbf{c} parameters to tune is still 72 (25+24+23) parameters for a 25-parameter retrieval. This was found to be too many parameters to robustly determine the constraint. For this reason, \mathbf{a} , \mathbf{b} , and \mathbf{c} were set to have a polynomial form in altitude. The order of the polynomial was chosen by considering 1) the order needed to optimize the figure of merit and 2) the stability of the fit.

Even with the fewer parameters, starting at different initial conditions with different scale factors resulted in somewhat different answers, more so for polynomial orders above 3. For this reason, the strengths were fit for polynomial 0 first, then updated as higher order polynomials were added sequentially. The non-robustness of this process leaves some question as to whether a global minimum was found; however the favorable comparisons to the climatological constraints shown in Table III, give confidence that a good result was found.

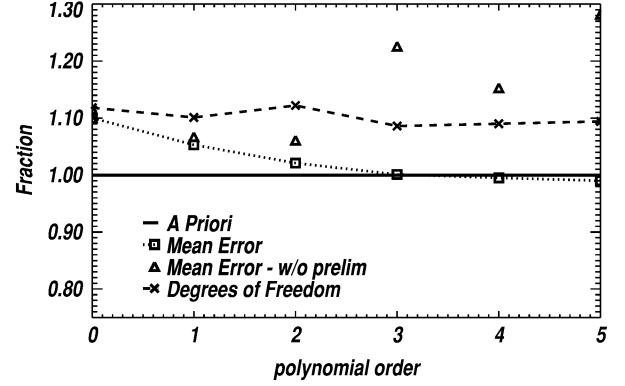


Fig. 3. Mean error and DOF for all species normalized by the results using climatological constraints. The red squares show the mean error when the parameters were fit sequentially by polynomial order, where the “initial” guess for order 1 is set to the best results for order 0. The purple triangles show the mean error when the parameters were fit by polynomial order without dependence on lower order polynomial results.

Fig. 3 shows the error and DOF for different polynomial orders for north midlatitude, 0–1 fit with figure of merit mean error/DOF^{1/8} for the MOZART dataset. This figure shows that there is minimal improvement over a third-order polynomial, and also shows the uncertainty of the fit increasing with polynomial order (Δ), especially beyond second order. The choice of polynomial order 3 was based on stability and tradeoff between DOF ($-x-$) and error ($-\square-$). The third-order polynomial results in about 0.1% higher mean error and about 9% more DOF than using the climatological constraints.

E. Constraint Solution

The necessary steps for finding the best height-dependent derivative constraint are as follows. 1) Compose the constraint from the current \mathbf{a} , \mathbf{b} , and \mathbf{c} parameters, as shown in (8). 2) Calculate the error covariance using (6) with this constraint. 3) Evaluate the result using the desired figure of merit, discussed in Section II-C. The solution method used was the Simplex Method [11], which does not require derivatives. The scale and step size were begun at a variety of values.

III. SETUP

A. Datasets

The following data sets were used as test datasets for constraint selection and testing. Covariances were created from each dataset for three latitude ranges: tropics (18S–18N), midlatitude (18N–54N), and polar (90S–54S).

1) *MOZART*: The MOZART dataset is from a run of the Model for Ozone And Related chemical Tracers (MOZART3) [12], [13]. We acquired one day’s worth of data for October 2 of an unspecified year which was used in the TES Single Orbit Test [14]. This dataset was interpolated from the 52 level native sigma grid to the TES standard grid (87 levels from 1211–0.1 mb). Pressure levels below the surface pressure supplied by MOZART were not used in the calculations.

2) *HARVARD/URAP*: For ozone, a climatology was created by combining the covariances of two datasets: the Harvard Climatology data based on ozonesonde measurements [15] which

covers pressure ranges 1000–10 mb smoothly combined and the URAP dataset is based on UARS measurements,² which covers pressure ranges 100 mb to the top of the TES atmosphere.

3) *GEOS-CHEM/MOZART*: For ozone and CO, climatologies were created by combining the covariances from two models. The covariance in the Troposphere (from the surface to one level above the tropopause, up to 68 mb) comes from profiles calculated using the Harvard GEOS-CHEM v5-07-08 model³ [17] simulating the year 2003. Covariance matrices were calculated using profiles for the months of September/October to coincide with the single day of MOZART profiles. The GEOS-CHEM covariance was combined with the same covariance from MOZART discussed above between 68 and 0.1 mB. There were no cross-correlations introduced between the MOZART and GEOS pressure regions.

4) *GMAO*: For water vapor, climatological constraints were created from a month's worth (August, 2005) of profiles from the NASA Goddard SFC–Global Modeling and Assimilation Office (GMAO) data products. The GMAO products were created using the GEOS-4 assimilation model “late look” product Bloom [18].⁴ The data was interpolated from the 36-level GMAO grid to the 87-level TES grid. Pressure levels below 1000 mb, the lowest GMAO pressure, were not used in the calculations.

B. Atmospheres for Constraint Selection

Constraints were selected for three different regions because of the large differences in temperature and trace gas composition between these regions: midlatitude, tropics, and polar. For each of these regions, one representative atmosphere was chosen to calculate the Jacobians used in (6). The location of the profiles are shown in Table I. The profiles for the Jacobian calculation are taken from a MOZART run for October 2 of an unspecified year [12], [13].

C. Measurement Frequencies and Noise

The measurement noise was computed from TES system test #5 and is described in Worden [3]. It is briefly shown in Table II.

D. Covariances

Covariances for the MOZART, Harvard, GEOS, and GMAO datasets were made by: 1) taking the logarithm of profiles for all species except T_{atm} ; 2) dividing the data into five bins (ARCTIC, 67N-90N; N_MIDLAT, 18N-67N; TROPICS, 18S-18N; S_MIDLAT, 67S-18S; and ANTARCTIC, 90S-67S); 4) Calculating the mean profile for each bin; and 5) finding the covariance of each bin with the mean profile subtracted.

E. Retrieval Strategy and Propagated Errors

The retrieval strategy includes retrieving species in a particular order. Retrieving all species at once can result in difficulty finding the global minimum. The retrieval order is: 1) T_{atm} and H_2O ; 2) O_3 ; 3) CO; and 4) CH_4 . Note that T_{atm} is always retrieved with the surface temperature, and emissivity is jointly

TABLE I
LOCATIONS FOR THE REPRESENTATIVE ATMOSPHERES
CHOSEN TO CALCULATE JACOBIANS

profile	latitude (deg.)	longitude (deg.)	solar time (H)
MIDLAT	46.3	-11.3	2.5
TROPICS	0.0	166.2	13.7
POLAR	-72.3	-148.2	16.4

TABLE II
BAND AVERAGE NESR VALUES USED FOR SIMULATED
MEASUREMENTS AND RETRIEVALS

TES Filter ID	Frequencies (cm^{-1})	Nadir NESR, 16 pixel avg. ($\text{nW/cm}^2/\text{sr/cm}^{-1}$)
2B1	650-900	133
1B2	950-1150	17
2A1	1100-1325	17
1A1	1900-2250	23

retrieved in all steps. When considering errors for T_{atm} , the full error covariance for a T_{atm} , H_2O , surface temperature, and emissivity retrieval is calculated, however the subcomponent of the error covariance corresponding to T_{atm} is pulled out.

With this strategy, the ozone retrieval assumes that H_2O and T_{atm} have already been retrieved and so \mathbf{S}_b , the uncertainty of H_2O and T_{atm} , is set to the retrieved error covariance in (6). The strategy assumes that CO and CH_4 have not yet been retrieved for the ozone step, and so \mathbf{S}_b is set to the *a priori* climatological covariance for CO and CH_4 .

F. Figure of Merit Choice

The figure of merit chooses the tradeoff between DOF and error. With the same error, more DOF are preferable. However, the relative value of minimizing error versus maximizing DOF is not obvious. Fig. 4 shows selected metrics (mean error, DOF, and resolution at 500 mb) for different figures of merit for the zeroth + first derivative constraints, normalized to results using climatological constraints. The results are grouped into species with fewer DOF [CO and CH_4 , Fig. 4(a)] and more DOF [H_2O , T_{atm} , and O_3 , Fig. 4(b)].

As expected, DOF and resolution worsen from left to right in Fig. 4, whereas the error improves, though much less significantly. For CO and CH_4 , which have a small number of DOF (averaging 0.64), the change in the number of DOF from $2\times$ to $0.6\times$ the *a priori* represents a change from an average 1.3–0.6 DOF. Fig. 4 was used to select the final figure of merit, mean error/ $\text{DOF}^{1/8}$. The choice of $1/8$ is arbitrary and depends on one's relative valuation of error and DOF. The same figure of merit was used for all species and regions although the relative contributions of DOF versus mean error to the figure of merit qualitatively changes with their relative sizes.

G. Derivative Choice

All combinations of zeroth, first, and second derivatives were tried. Fig. 5 shows that all types performed adequately, with the zeroth+second derivatives performing best (lowest mean error and highest DOF), followed closely by zeroth + first derivatives. For TES retrievals, zeroth + first derivatives were chosen because it was an extension of the previously used first derivative

²<http://hyperion.gsfc.nasa.gov/Analysis/UARS/urap/home.html>

³<http://www-as.harvard.edu/chemistry/trop/geos/index.html>

⁴<http://gmao.gsfc.nasa.gov/systems/geos4>

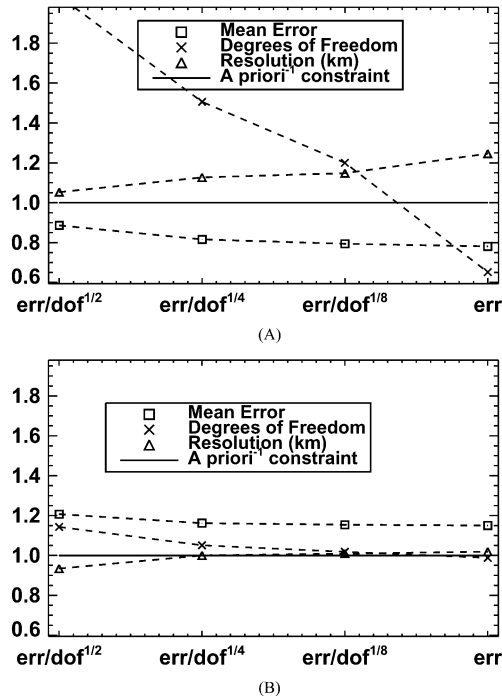


Fig. 4. Selecting the figure of merit. Mean error, DOF, and resolution at 500 mb averaged over all regions and species for CO and CH₄ (panel A) and T_{atm}, H₂O, and O₃ (panel B) normalized by the results using climatological constraints. As the figure of merit weights DOF more (toward left of plots), the DOF are greater, but the mean error is also higher. This is especially noticeable for species with fewer DOF (panel A).

constraints described by [9]. The rest of this paper focuses on zeroth + first derivative constraints, although the results should extend to zeroth+second derivative constraints. This figure also shows why, as previously discussed, the resolution at 500 mb is not a good figure of merit. Although the total DOF throughout the atmosphere have improved compared to the climatological constraints, the resolution at 500 mb has worsened.

IV. RESULTS

A. Average Results by Species

Altitude-dependent constraints were constructed for T_{atm}, H₂O, O₃, CO, and CH₄ for three different climatological regions (mid-latitude, tropics, and polar) using the MOZART climatology and the figure of merit mean error/DOF^{1/8}. To assess these constraints, metrics are calculated and compared to the climatological constraint results in Table III.

Table III shows that the temperature results have 0.6 K more error when the altitude-dependent derivative constraints are used, as compared to the climatological constraints, although temperature retrievals also have 1.2 more DOF and better resolution at 500 mB. Choosing a figure of merit that considers only *mean error* would improve the temperature error result for the altitude-dependent constraints.

Water vapor results have better mean error than the climatological constraint results. This was found to result from large systematic and cross-state errors for water vapor. However, the altitude-dependent results also have less DOF for water vapor (3.75 versus 4.93). Note that the mean error is averaged over

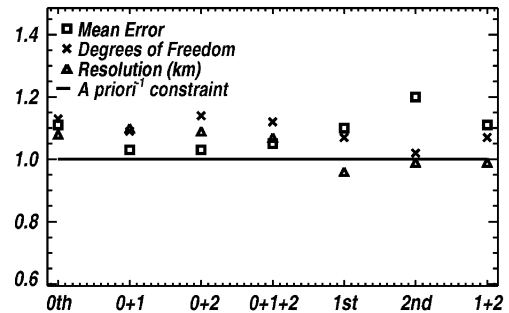


Fig. 5. Selecting constraint derivative type. The various metrics are shown averaged over all species and regions normalized by the results using the climatological constraints. This figure shows that, for example, zeroth and first derivative constraints “0 + 1” has slightly more mean error (1.02) than the climatological constraint errors, but also have about 9% more DOF, on average.

TABLE III
(a) INITIAL MEAN ERROR. (b) RESULTS FOR ALTITUDE-DEPENDENT CONSTRAINTS. (c) RESULTS FOR CLIMATOLOGICAL

	T _{atm}	H ₂ O	O ₃	CO	CH ₄
Init. mean error	4.6K	0.39	0.39	0.19	0.05

(a)

	T _{atm}	H ₂ O	O ₃	CO	CH ₄
Figure of merit	1.70	0.16	0.24	0.16	0.05
Mean error	2.2K	0.19	0.29	0.17	0.04
Deg. freedom	7.76	3.75	5.13	1.29	0.38
Resolution (km)	4.5	2.9	6.3	8.9	10.1

(b)

	T _{atm}	H ₂ O	O ₃	CO	CH ₄
Figure of merit	1.26	0.17	0.22	0.17	0.08
Mean error	1.6K	0.21	0.27	0.16	0.07
Deg. freedom	6.58	4.93	4.58	0.68	0.60
Resolution (km)	5.0	2.6	6.5	8.9	8.9

(c)

the entire water vapor profile, including the stratosphere where TES is not sensitive. The difference between a mean error of 0.19 versus 0.21 is correspondingly more significant than the 0.02 difference.

Ozone shows only modest differences between the two results. However, CO shows an increase in DOF from 0.68 to 1.29 traded for about a 1% increase in mean error.

The CO increase in DOF occurs in the polar region, where the climatological constraint constrains CO to 0.13 DOF with no improvement on the *a priori* error (which has a mean error of 2.9%). The altitude-dependent constraints result in 0.43 DOF and mean error 3.0%. If the polar region is excluded, the improvement relative to *a priori* constraint results is more modest, only a 9% improvement in DOF rather. Polar CO is excluded from the comparisons between GEOS and MOZART in Table IV.

Note that the figure of merit for this study could have been chosen as *mean error* instead of mean error/DOF^{1/8}, which would result in better error results at the expense of DOF. The choice of the figure of merit depends on the user’s preferences.

B. Example Constraint Strengths

The strength parameters for the combined zeroth and first derivatives are allowed to vary independently. In some cases,

TABLE IV
RATIO OF MEAN ERRORS FOR EXPECTED AND UNEXPECTED CLIMATOLOGIES

(a)			
O_3	MOZART	HARVARD/URAP	
MOZART	1.07 \pm 0.05	0.93 \pm 0.06	
HARVARD/URAP	0.77 \pm 0.08	1.06 \pm 0.18	
(b)			
O_3	MOZART	GEOS/MOZART	
MOZART	1.07 \pm 0.05	0.97 \pm 0.14	
GEOS/MOZART	0.87 \pm 0.14	1.21 \pm 0.39	
(c)			
CO	MOZART	GEOS/MOZART	
MOZART	1.05 \pm 0.05	1.02 \pm 0.08	
GEOS/MOZART	1.00 \pm 0.06	1.08 \pm 0.04	
(d)			
H_2O	MOZART	GMAO	
MOZART	0.92 \pm 0.20	0.97 \pm 0.10	
GMAO	0.44 \pm 0.34	1.01 \pm 0.27	

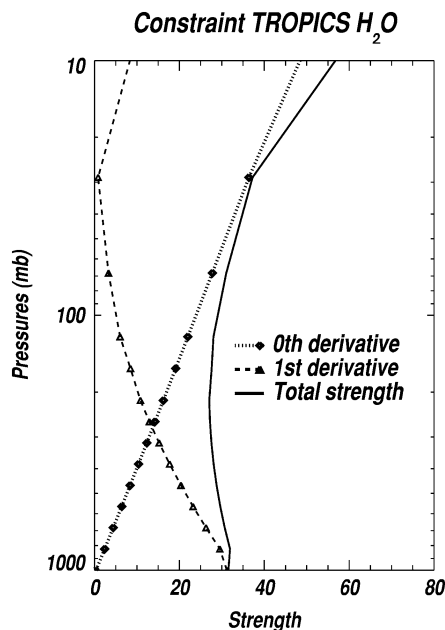


Fig. 6. Relative strengths of the zeroth and first derivative altitude-dependent constraint for H_2O . The constraint matrix is dominated by the first derivative in the troposphere, where TES has sensitivity to H_2O . In the stratosphere, however, the constraint is dominated by the zeroth derivative which results in H_2O remaining at the *a priori* value, as shown in Fig. 7.

like stratospheric water vapor for which TES has no sensitivity, we expect the constraint to be strong and dominated by zeroth derivative; in other cases, like tropospheric water, we expect the constraint strengths to be dominated more by the first derivative. Fig. 6 shows the constraint strengths for TROPICS water vapor. The constraint strengths behave as expected, with water vapor heavily dominated by the zeroth derivative in the stratosphere and by the first derivative in the troposphere.

C. Example Retrieval Using Altitude-Dependent Constraints

A retrieval example with the TES nonlinear algorithm is shown for water vapor in Fig. 7. The first derivative single

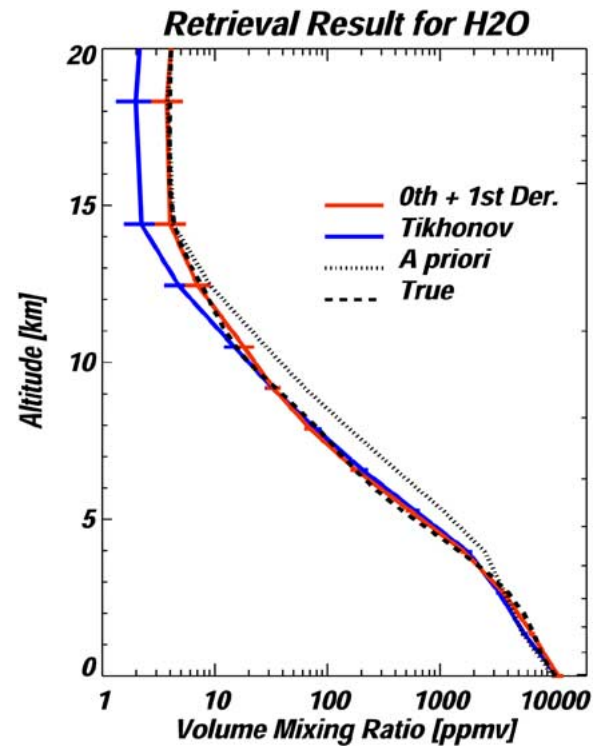


Fig. 7. Retrieval results using a single-strength first derivative Tikhonov constraint (blue), and an altitude-dependent zeroth + first derivative constraint described in this paper (red). The solid line shows the retrieval result, the dashed line shows the true, and the dotted line the *a priori*. The horizontal bars show the predicted total error at the retrieval levels.

strength constraint as described in Steck [9] is compared to the altitude-dependent zeroth + first derivative constraint described in this paper. This single retrieval example is only a demonstration, but it does show how the altitude-dependent constraint result returns to the *a priori* in the stratosphere (where there is little information or variability), whereas the first derivative single strength constraint result follows the shape of the *a priori*, leading it away from the *a priori* in the stratosphere in this particular case.

The averaging kernel (\mathbf{A}), shown in Fig. 8, gives a clearer picture of the retrieval characterization than a single retrieval result. The left panel shows \mathbf{A} for the first derivative single strength constraint; the right for the new altitude-dependent constraint. The left panel averaging kernel indicates that the retrieved stratospheric values (parameters 10–13) are correlated with the true state values of parameters 8 and 9. This results in the retrieval example seen in Fig. 8, which shows the retrieved values of parameters 10–12 tracking the *slope* of the prior. In contrast, the altitude-dependent Tikhonov averaging kernel indicates that little or no information from the true state is reported in the retrieved values, and consequently the retrieval tracks the prior *value*.

D. Constraints Applied to an Unexpected Climatology

The climatology that is used to create the constraint matrix will likely differ from the actual climatology. To test the effect

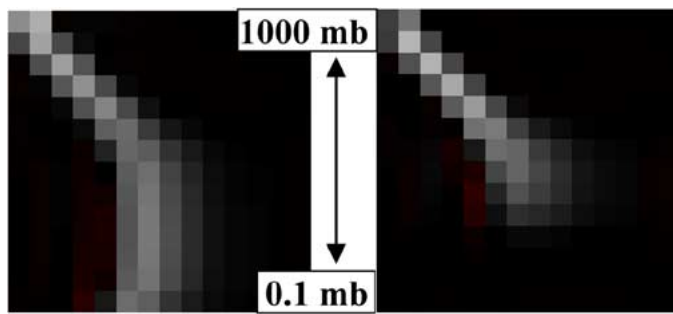


Fig. 8. Comparison of averaging kernels for a single-parameter first-derivative Tikhonov constraint (left), and a zeroth + first derivative altitude-dependent constraint (right). The plot shows the 14 retrieved water vapor values which are located between 1000 and 0.1 mb, with $A_{1,1}$ at the upper left corner and $A_{14,14}$ at the lower right corner of the figure. White values indicate that the retrieved value is correlated to the true value, red values indicate that the retrieved value is anticorrelated to the true value, and black indicates no correlation. (white = +0.8, black = 0, red = -0.8).

of using an assumed climatology that is different than the actual climatology, constraints were developed using the MOZART climatology and applied to another equally valid climatology, and vice versa. Gaussian statistics are assumed in both cases, but this assumption was not explored. For ozone, MOZART was compared to HARVARD/URAP and GEOS-CHEM/MOZART. For CO, MOZART was compared to GEOS-CHEM/MOZART. For water vapor, MOZART was compared to GMAO. Table IV shows the relative performance of the altitude-dependent derivative constraints to the climatological constraints for these cases, averaged over all three latitude regions.

Although the differences are modest, the altitude-dependent constraint on average does not do as well as the climatological constraint when the actual and assumed climatologies are the same, as seen by the diagonal entries in Table IV which are almost all greater than 1. However, a modest improvement over the climatological constraint is seen when the actual and assumed climatologies differ, as seen by the off-diagonal entries in Table IV. The off-diagonal entries are consistently less than 1 for Ozone and H₂O, and are improved for CO relative to the diagonals. This indicates that, on average, the altitude-dependent constraints have a more robust response to an uncertain climatology.

V. CONCLUSION

A method for creating altitude-dependent derivative constraints for the trace gas retrievals was presented. The technique was based on the optimization of a figure of merit, which can include *a posteriori* error and DOF, and uses a constraint that is composed of combinations of the zeroth-, first-, and second-order Tikhonov constraints with altitude-dependent weights.

Four different datasets (GMAO, MOZART, HARVARD/URAP, and GEOS-CHEM) were selected to construct and test the constraints for TES retrievals of atmospheric CO, H₂O, O₃, CH₄, and temperature. The retrieval errors obtained using the altitude-dependent constraints on the MOZART climatology were comparable to the retrieval errors obtained from inverse

climatological covariances calculated directly from the dataset. For O₃, CO, and H₂O mean retrievals errors differed by 10% or less (i.e., ranging from 0.9 to 1.1 times the error resulting from the climatological constraint). The largest changes were observed for the CH₄ and temperature retrievals; the retrieval error for CH₄ decreased by 50%, whereas the mean error for the temperature retrieval increased by 37% (i.e., 1.37 times the error resulting from the climatological constraint), which is due partly to a figure of merit that included DOF in addition to the retrieval error.

The altitude-dependent derivative constraints were found to be more robust than the climatological constraint when the incorrect climatology was specified. When a climatological constraint was constructed from a one of the four datasets and applied to a climatology derived from a different dataset, the mean retrieval error was modestly but consistently better than that obtained with the climatological constraint. For example, a large reduction (23%) in the estimated retrieval error was seen for O₃ when the altitude-dependent derivative constraint was created from the HARVARD/URAP dataset and applied to a climatology based on the MOZART dataset, as compared to the climatological constraint created from the HARVARD/URAP dataset and applied to the MOZART dataset.

An important feature of this approach, in contrast to a single strength first derivative Tikhonov constraint, is that retrievals revert to the *a priori* profile in regions of the atmosphere where the observations are insensitive. For example, retrievals of H₂O revert to the *a priori* profile in the stratosphere where water vapor abundances have little impact on TES infrared spectral radiances, whereas a first derivative Tikhonov constraint can modify the stratospheric H₂O estimates based on correlations to the troposphere.

This technique is currently being used operationally for the TES retrievals of water vapor, CO, and CH₄. For results with these constraints over one orbit of simulated data, see Kulawik *et al.* [14].

ACKNOWLEDGMENT

The authors would like to thank J. Logan, T. Clough, C. Rodgers, T. Steck, the TES science team, and the TES software team.

REFERENCES

- [1] H. W. Engl, M. Hanke, and A. Neubauer, *Regularization of Inverse Problems*. Norwell, MA: Kluwer, 1996.
- [2] C. D. Rodgers, *Inverse Methods for Atmospheric Sounding: Theory and Practice*, Singapore: World Scientific, 2000.
- [3] J. Worden, S. S. Kulawik, M. W. Shephard, S. A. Clough, H. Worden, K. Bowman, and A. Goldman, "Predicted errors of Tropospheric Emission Spectrometer nadir retrievals from spectral window selection," *J. Geophys. Res.*, vol. 109, no. D9, May 15, 2004.
- [4] R. Beer, T. Glavich, and D. Rider, "Tropospheric Emission Spectrometer for the Earth Observing System's Aura satellite," *Appl. Opt.*, vol. 40, pp. 2356–2367, 2001.
- [5] K. W. Bowman, C. D. Rodgers, S. S. Kulawik, J. Worden, E. Sarkissian, G. Osterman, T. Steck, M. Lou, A. Eldering, M. Shephard, H. Worden, M. Lampel, S. Clough, P. Brown, C. Rinsland, M. Gunson, and R. Beer, "Tropospheric Emission Spectrometer: Retrieval method and error analysis," *IEEE Trans. Geosci. Remote Sens.*, vol. 44, no. 5, pp. 1297–1307, May 2006.

- [6] T. von Clarmann, U. Grabowski, and M. Kiefer, "On the role of non-random errors in inverse problems in radiative transfer and other applications," *J. Quant. Spectrosc. Radiat. Transf.*, vol. 71, no. 1, pp. 39–46, Oct. 1, 2001.
- [7] W. Menke, *Geophysical Data Analysis: Discrete Inverse Theory*. New York: Academic, 1989.
- [8] A. Tikhonov, "On the solution of incorrectly stated problems and a method of regularization," *Dokl. Acad. Nauk SSSR*, vol. 151, pp. 501–504, 1963.
- [9] T. Steck, "Methods for determining regularization for atmospheric retrieval problems," *Appl. Opt.*, vol. 41, pp. 1788–1797, Mar. 20, 2002.
- [10] A. Doicu, F. Schreier, and M. Hess, "Iterative regularization methods for atmospheric remote sensing," *J. Quant. Spectrosc. Radiat. Transf.*, vol. 83, pp. 47–61, 2004.
- [11] J. A. Nelder and R. Mead, "A simplex-method for function minimization," *Comput. J.*, vol. 7, pp. 308–313, 1965.
- [12] G. P. Brasseur, D. A. Hauglustaine, S. Walters, P. J. Rasch, J. F. Muller, C. Granier, and X. X. Tie, "MOZART, a global chemical transport model for ozone and related chemical tracers 1. Model description," *J. Geophys. Res.—Atmos.*, vol. 103, pp. 28 265–28 289, 1998.
- [13] M. Park, W. J. Randel, D. E. Kinnison, R. R. Garcia, and W. Choi, "Seasonal variation of methane, water vapor, and nitrogen oxides near the tropopause: Satellite observations and model simulations," *J. Geophys. Res.—Atmos.*, vol. 109, no. D3, 2004. DOI: 10.1029/2003JD003706.
- [14] S. S. Kulawik, H. Worden, G. Osterman, M. Luo, R. Beer, D. Kinnison, K. W. Bowman, J. Worden, A. Eldering, M. Lampel, T. Steck, and C. Rodgers, "TES atmospheric profile retrieval characterization: An orbit of simulated observations," *IEEE Trans. Geosci. Remote Sens.*, vol. 44, no. 5, pp. 1324–1333, May 2006.
- [15] J. A. Logan, "An analysis of ozonesonde data for the troposphere: Recommendations for testing 3-D models, and development of a gridded climatology for tropospheric ozone," *J. Geophys. Res.*, vol. 104, pp. 16 115–16 149, 1999.
- [16] J. A. Logan, "An analysis of ozonesonde data for the lower stratosphere: Recommendations for testing models," *J. Geophys. Res.*, vol. 104, pp. 16 151–16 170, 1999.
- [17] I. Bey, D. J. Jacob, R. M. Yantosca, J. A. Logan, B. D. Field, A. M. Fiore, Q. B. Li, H. G. Y. Liu, L. J. Mickley, and M. G. Schultz, "Global modeling of tropospheric chemistry with assimilated meteorology: Model description and evaluation," *J. Geophys. Res.—Atmos.*, vol. 106, no. D19, pp. 23 073–23 095, 2001.
- [18] S. Bloom, A. da Silva, D. Dee, M. Bosilovich, J.-D. Chern, S. Pawson, S. Schubert, M. Sienkiewicz, I. Stajner, W.-W. Tan, and M.-L. Wu, "Documentation and validation of the Goddard Earth Observing System (GEOS) data assimilation system—Version 4," NASA Goddard Space Flight Center, Greenbelt, MD, Tech. Rep. Ser. Global Modeling and Data Assimilation 104606, 2005.



Susan Sund Kulawik received the B.S. degree from The Ohio State University, Columbus, in 1991 and the Ph.D. in physics from the University of Michigan, Ann Arbor, in 1999.

She is a member of the Tropospheric Emission Spectrometer (TES) Science Team and has worked on TES since 1999, first at Raytheon ITSS in Pasadena, CA, and at the Jet Propulsion Laboratory, Pasadena, since 2002. Her research interests include the use of information theory to select constraints and spectral windows, error analysis, retrievals in

the presence of clouds, and HNO_3 retrievals from TES data.



Gregory Osterman received the B.S. degree in physics from Texas A&M University, College Station, in 1987, the M.S. degree in physics from Texas Tech University, Austin, and the Ph.D. degree in physics from the University of Texas at Dallas, Richardson, in 1994.

He is a member of the Tropospheric Emission Spectrometer (TES) Science Team, Jet Propulsion Laboratory, Pasadena, CA, and focuses primarily on validation of TES data. His research interests also include studying tropospheric ozone using TES and

other data sources as well as models.



Kevin W. Bowman received the B.E.E. degree in electrical engineering from Auburn University, Auburn, AL, the Diplome de Specialization en Traitement et Transmission des Informations from the Ecole Superieure d'Electricite (SUPELEC), Metz, France, and the M.S. and Ph.D. degrees in electrical engineering at the Georgia Institute of Technology, Atlanta, in 1991, 1992, 1993, and 1997, respectively.

He has been a Member of the Technical Staff at the Jet Propulsion Laboratory, Pasadena, CA, since 1997.

His primary research interests are in the area of atmospheric remote sensing and tropospheric chemistry including inverse modeling and data assimilation from satellite observations, estimation and error analysis of trace gas profiles, and calibration algorithms for infrared Fourier transform spectrometers.



Dylan B. A. Jones received the B.A. degree in physics and astrophysics, the M.Sc. degree in applied physics, and the Ph.D. degree in earth and planetary science from Harvard University, Cambridge, MA.

He is an assistant professor in the Department of Physics at the University of Toronto, Toronto, ON, Canada. His research is focused is on understanding how pollution influences the dynamical and chemical state of the atmosphere, using satellite measurements of atmospheric trace gases together with global

three-dimensional modeling of tropospheric chemistry and transport, inverse modeling, and chemical data assimilation.